XI. PLASMA PHYSICS*

Prof. S. C. Brown
Prof. G. Bekefi
Prof. D. R. Whitehouse
M. L. Andrews
V. Arunasalam
C. D. Buntschuh
J. F. Clarke
J. D. Coccoli
F. X. Crist
E. W. Fitzgerald, Jr.
W. H. Glenn, Jr.
E. B. Hooper, Jr.
J. C. Ingraham
P. W. Jameson
R. L. Kronquist
D. T. Llewellyn-Jones
J. J. McCarthy
W. J. Mulligan
J. J. Nolan, Jr.
H. R. Radoski
G. L. Rogoff
F. Y-F. Tse
R. E. Whitney

A. EXCITATION OF THE OPTICAL SPECTRUM IN THE HOLLOW-CATHODE ARC

1. Introduction

The intensity of a spectral line from a unit volume of plasma, with self-absorption and broadening neglected, is given by

$$I_{jk} = n_j A_{jk} h\nu_{jk}, \tag{1}$$

where n_j is the density of emitting atoms or ions in the j^{th} excited state, A_{jk} is the transition probability from the j^{th} state to the k^{th} state, and $h\nu_{jk}$ is the photon energy. In a low-pressure arc plasma, which is far from thermal equilibrium, it is necessary to consider the rates of the various populating processes in order to arrive at an expression for n_j in terms of the plasma properties.

The plasma that we are studying is a highly ionized argon arc.[1] The base pressure before ionization is a few μ Hg. The electron density is of the order of 10^{13} cm^{-3}; electron temperatures are several volts at the center of the column. Ion temperatures may be one volt, or more.[2] The spectrum from 3200 Å to 5200 Å contains, for the most part, AII lines and several weak AI and AIII lines.

In a plasma the population process is frequently predominantly electronic excitation from the ground state, and the depopulation process is principally spontaneous emission to all lower states. In this case,

$$n_j = \frac{\beta_{oj} n_o n_-}{A_j}, \tag{2}$$

where β_{oj} is the excitation coefficient, n_o is the density of atoms or ions in the ground state, and A_j is the transition probability per second to all lower states. We shall use

*This work was supported in part by the U. S. Atomic Energy Commission (Contract AT(30-1)-1842); and in part by the U. S. Air Force (Electronic Systems Division) under Contract AF19(604)-5992.

this expression in analyzing the data; however, for the conditions obtaining in the arc, radiative recombination, stepwise electronic excitation, and cascading may give significant contributions to n_j. In this report we consider these other processes and estimate their rates relative to electronic excitation. We shall find that the competing processes may have rates comparable to, but somewhat smaller than, electronic excitation, so that Eq. 2 represents a reasonably good approximation.

In plasmas at micron pressures there is negligible self-absorption of nonresonance radiation at optical frequencies, and negligible population by collisions of the second kind. We shall also neglect the effects of metastables. This is probably not legitimate for the argon atom. If the ion has any metastable levels, they are probably close enough to the radiating levels (less than T_+) to be considered as merged into a single radiating state. Throughout this report a Maxwellian electron distribution is assumed. This is reasonable in view of the high electron temperatures and high degree of ionization. Because none of the relevant cross sections and atomic constants are available for the argon ion, and very few for the atom, it has been necessary to make order-of-magnitude guesses of the values.

2. Excitation Coefficients

The coefficient β_{ij} for excitation from the i^{th} to the j^{th} state by electron impact is the average over the electron distribution function of the cross section σ_{ij} multiplied by the electron velocity v. For a Maxwellian at temperature T_- volts,

$$\beta_{ij} = \sqrt{\frac{8eT_-}{\pi m}} \int_{V_x/T_-}^{-\infty} \sigma_{ij}(u) \frac{u}{T_-} e^{-u/T_-} d\frac{u}{T_-}, \tag{3}$$

where u is the electron energy, and $V_x = V_j - V_i$ is the difference in excitation potential. The ionization coefficient $\beta_{o\infty}$ is also given by Eq. 3.

There are very limited data on the cross sections, especially for argon. There are no data for the excitation or ionization from the ground state of the ion, or from higher levels of either the atom or ion. We can obtain a useful approximation by noting that all of the cross sections have the general form shown by the solid line in Fig. XI-1. For excitation, σ_m is of the order of 10^{-19} cm^2, and V_m is slightly greater than V_x. For ionization, $\sigma_m \sim 10^{-16}$ cm^2, and V_m is several times V_∞, the ionization potential. Three approximations to $\sigma(u)$ which permit Eq. 3 to be readily integrated are shown as dotted lines:

$$\left.\begin{aligned} \sigma_1 &= c_1/u \\ \sigma_2 &= c_2(u-V_x) \\ \sigma_3 &= \sigma_m \end{aligned}\right\} \qquad u > V_x$$

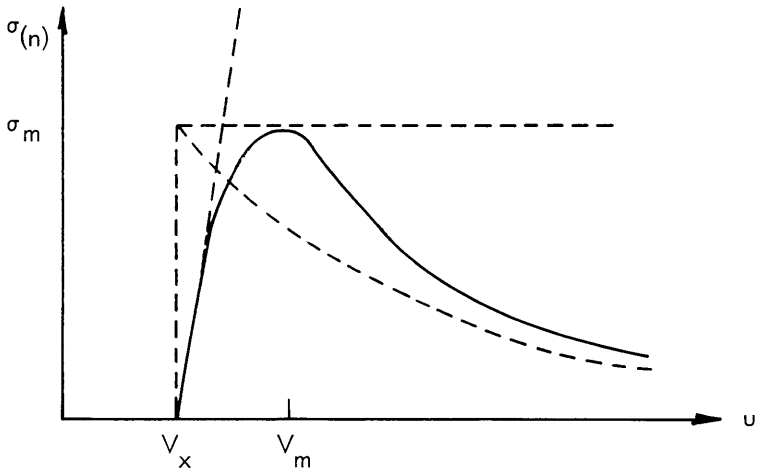

Fig. XI-1. Approximate excitation and ionization cross sections.

For σ_1, we use the theoretical formula $\sigma = C(\ln u)/u$, suppressing the slowly varying logarithm.[3] σ_2 is the popular approximation for low T; σ_3 improves on this for higher T. The resulting coefficients, in mks units, are

$$\beta_1 = C_1 \sqrt{\frac{8e}{\pi m}}\, T_-^{-1/2}\, e^{-V_x/T_-}$$

$$\beta_2 = C_2 V_x \sqrt{\frac{8e}{\pi m}} \left(1 + \frac{2T_-}{V_x}\right) T_-^{-1/2}\, e^{-V_x/T_-}$$

$$\beta_3 = \sigma_m V_x \sqrt{\frac{8e}{\pi m}} \left(1 + \frac{T_-}{V_x}\right) T_-^{-1/2}\, e^{-V_x/T_-}.$$

At low electron temperatures the exponent contains the principal variation of β with T_-, and it makes little difference which coefficient is used. At high temperatures, the first expression, which takes into account the decreasing cross section at high energy, is presumably the best approximation. For this reason, we use β_1, choosing $C_1 = \sigma_m V_\infty$.

For argon atoms, $V_\infty = 15.8$ volts, we have

$$\beta_{ij}^o = 1.1 \times 10^{-10} T^{-1/2}\, e^{-V_x/T}\ \text{cm}^3/\text{sec}. \tag{4a}$$

$$\beta_{o\infty}^o = 1.1 \times 10^{-7} T^{-1/2}\, e^{-15.8/T}. \tag{4b}$$

For argon ions, $V_\infty = 27.5$ volts, we have

$$\beta_{ij}^{+} = 1.8 \times 10^{-10} T^{-1/2} \, e^{-V_x/T} \tag{4c}$$

$$\beta_{o\infty}^{+} = 1.8 \times 10^{-7} T^{-1/2} \, e^{-27.5/T}. \tag{4d}$$

The average cross sections for excitation and ionization of an atom already in an excited state (for example, the resonance level) seem to be an order of magnitude greater than those of an atom in the ground state.[3] For the most part, this is due to the fact that $V_j - V_i$ is much smaller than $V_j - V_o$. Possibly there is an increase in σ_m because of the greater size of the excited atom, but for order-of-magnitude estimates we shall ignore this possibility.

3. Densities of Singly and Doubly Ionized Ions

It is necessary to know the densities of neutrals, singly and doubly ionized ions, and electrons in order to compute the rate of excitation from the ground state and rate of volume recombination. To estimate these densities, consider the following model. The atom has first and second ionization potentials V_1 and V_2, respectively. Neglect excitation and higher degrees of ionization. Suppose that ions are generated only by electron impact from the ground state, that is, $A \rightarrow A^+$ and $A^+ \rightarrow A^{++}$, with ionization coefficients β^o and β^+, respectively. Assume that recombination is at the walls, with a time constant τ for either ion.

In the steady state, the particle balance equations are

$$\begin{aligned}
\frac{dn_o}{dt} &= 0 = \frac{1}{\tau}(n_+ + n_{++}) - \beta^o n_- n_o \\
\frac{dn_+}{dt} &= 0 = \beta^o n_- n_o - \left(\frac{1}{\tau} + \beta^+ n_-\right) n_+ \\
\frac{dn_{++}}{dt} &= 0 = \beta^+ n_- n_+ - \frac{1}{\tau} n_{++}.
\end{aligned} \tag{5}$$

The total heavy-particle concentration $N = n_o + n_+ + n_{++}$ is fixed; charge neutrality requires $n_- = n_+ + 2n_{++}$. Solving Eqs. 5, subject to these constraints, yields

$$\begin{aligned}
\frac{n_-}{N} &= \left[1 - \frac{k_1 + k_2}{2Nk_1k_2}\right] + \sqrt{\left[1 - \frac{k_1 + k_2}{2Nk_1k_2}\right]^2 + \frac{Nk_1 - 1}{N^2 k_1 k_2}} \\
\frac{n_o}{N} &= \frac{1}{1 + k_1 n_-} \\
\frac{n_+}{N} &= \frac{k_1 n_-}{(1 + k_2 n_-)(1 + k_1 n_-)}; \qquad \frac{n_{++}}{N} = \frac{k_1 k_2 n_-^2}{(1 + k_2 n_-)(1 + k_1 n_-)},
\end{aligned} \tag{6}$$

where $k_1 = \beta^o\tau$, $k_2 = \beta^+\tau$.

The excitation coefficients are given in Eq. 4b and 4d. The mean loss time for ions is difficult to evaluate. It must be somewhere between the free-flight loss time to the ends of the arc column and the radial diffusion time across the magnetic field. In the arc, this is between 10^{-5} and 10^{-2} sec. In Fig. XI-2, n_o, n_+, and n_{++} are plotted for $\tau = 10^{-3}$ and 10^{-4} sec, respectively, for $N = 10^{14}$ cm^3. If triply ionized atoms were included, the n_{++} density would reach a maximum and then fall off, and n_{+++} would build up as T_- increases. It is important to note that for T_- just roughly 0.5 volt above threshold, n_{++}/n_+ is 5-15 per cent, which value is an appreciable fraction of the total ionization.

The actual operating point of the arc can be varied by adjusting the arc current, gas-flow rate, and magnetic field. It should also be remembered that the plasma is also generated inside the hollow cathode where the density and temperature are much higher. It is, therefore, quite possible that the electron temperature in the positive column is somewhat lower than that calculated on this model for a given electron density.

4. Imprisonment of Resonance Radiation

If resonance radiation is strongly absorbed by atoms or ions in the ground state, it is imprisoned and leads to increased population of the resonance levels. Here we take the resonance levels to be the lower excited states, and neglect the higher states that have alternate transitions available. To estimate the degree of imprisonment, let the excitation of a resonance level be by electron impact and photon absorption, and let de-excitation by all processes except spontaneous emission have a time constant τ_d. Then, the balance equations for atoms in the resonance level and photons are

$$\frac{dn_1}{dt} = 0 = \beta_{o1} n_o n_- + B\rho n_o - \frac{n_1}{\tau_d} - An_1 \tag{7}$$

$$\frac{dn_\nu}{dt} = 0 = An_1 - B\rho n_o - \frac{n_\nu}{\tau_\nu}, \tag{8}$$

where A and B are the Einstein coefficients, ρ is the monochromatic energy density for resonance radiation, n_1 is the resonance level population, n_ν is the total photon density in the line, and τ_ν is the photon escape time. We shall approximate ρ by $n_\nu h\nu/\Delta\nu_D$, where $\Delta\nu_D = \frac{\nu}{c}\sqrt{\frac{2kT_o}{M}}$ is the Doppler width of the line.

Holstein[4] has given an expression for τ_ν in the limit of large absorption for cylindrical geometry and Doppler-broadened radiation:

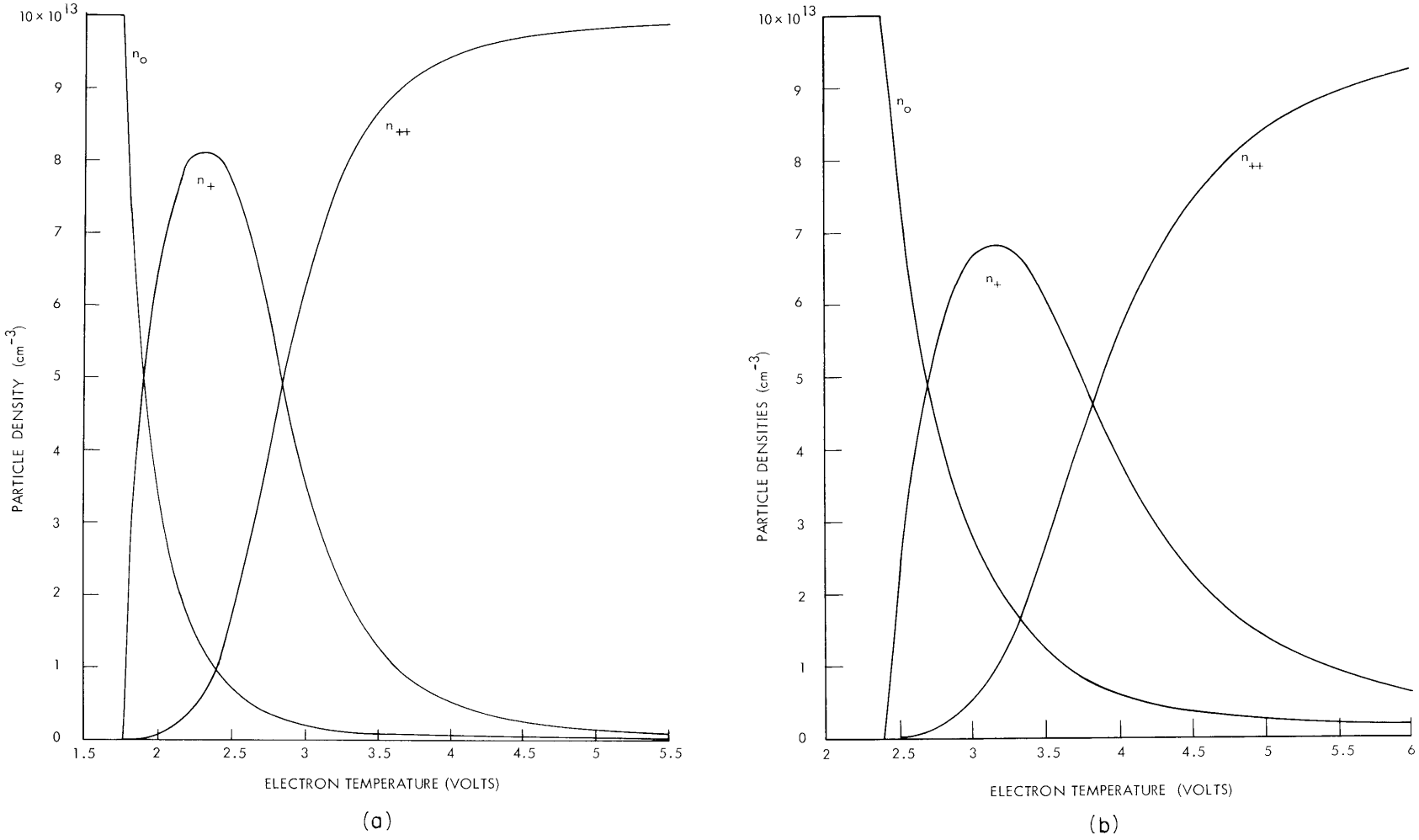

Fig. XI-2. Particle densities in highly ionized plasmas. (a) Ion loss time $\tau = 10^{-3}$ sec. (b) Ion loss time $\tau = 10^{-4}$ sec.

$$\tau_\nu = \frac{k_o R \sqrt{\pi \ln k_o R}}{1.6A}, \tag{9}$$

where

$$k_o = \frac{1}{8\pi^{3/2}} \frac{c^2}{\nu^2} \frac{Ag_1}{g_o} \frac{n_o}{\Delta\nu_D} \tag{10}$$

is the absorption coefficient at the center of the line.

If we introduce into Eq. 7 an imprisonment factor defined by the ratio of absorption to emission, $\mathcal{I} = B\rho n_o/An_1$, we can see that the density n_1 is governed by spontaneous emission, or other processes accordingly as $(1-\mathcal{I})A\tau_d$ is much greater or much less than one. From Eqs. 8-10 and the ratio of Einstein coefficients, we obtain

$$\mathcal{I} = \frac{1}{1 + c\frac{T_o}{n_o^2}}, \tag{11}$$

where $c = 2.3 \times 10^{24}$ cm^{-6} volt^{-1} for both neutrals and ions, if we take $A = 5 \times 10^7$ sec^{-1}, $g_o/g_1 = 1/4$, $\lambda = 1050$ Å for the atom, and $A = 6.6 \times 10^8$ sec^{-1}, $g_o/g_1 = 1$, $\lambda = 700$ Å for the ion (rather arbitrarily), and $R = 3$ cm, $\sqrt{\ln k_o R} = 2$. The transition probabilities are uncertain, but are probably of the correct order of magnitude.

The value of $1 - \mathcal{I}$ for ions in the arc is roughly bracketed by 9×10^{-5} ($T_+ = 2^V$, $n_+ = 10^{13}$ cm) and 4.5×10^{-2} ($T_+ = 0.1^V$, $n_+ = 5 \times 10^{13}$ cm^3). The other principal depopulating processes are likely to be either superelastic or ionizing collisions with electrons. For these, τ_d may be between 10^{-4} and 10^{-5} sec. Thus we might expect $(1-\mathcal{I})A\tau_d$ to be between 0.6 and 3×10^3. This means that the imprisonment is generally not quite great enough for us to neglect spontaneous emission as a depopulating process as compared with the other losses, but it is enough to decrease the effective transition probability by several orders of magnitude.

5. Competing Processes

We now consider the relative rates of excitation and de-excitation of a nonresonant level. Neglect photon absorption and populating collisions of the second kind. Assume that stepwise excitation is from the resonant level only, and that cascading is from a single upper level. The balance equation is

$$\frac{dn_j}{dt} = 0 = \beta_{oj} n_- n_o + \beta_{1j} n_- n_1 + A_{kj} n_k + \alpha_j n_\infty n_- - n_j[A_j + \tau_{d_j} + \tau_{c_j} + \beta_{jk} n_- + \beta_{j\infty} n_-], \tag{12}$$

where n_o, n_1, n_j, n_k are the populations of the ground, resonant, radiating, and cascading levels, respectively; n_∞ is the ground-state density of ions of next higher degree; α_j is the recombination coefficient; and τ_{d_j} and τ_{c_j} are the mean times for escape from the plasma and collisions of the second kind, respectively. Typical values of all coefficients are given in Table XI-1 for the argon ion, with $V_1 = 16^V$, $V_j = 20^V$, $V_k = 22^V$, and $V_\infty = 27.5^V$.

It is quite apparent that the upper levels de-excite almost exclusively by spontaneous emission, as expected.

Radiative recombination is the only significant volume recombination process in the arc. The partial coefficient for recombination to an individual level decreases rapidly with distance above the ground state, especially when the electron energy is high.[5] The formula $\alpha_j = 10^{-13} T^{-3/4}$ represents only a crude estimate based on calculations for monatomic hydrogen.[3,5] In Table XI-2 we give the ratio of recombination rate to electron excitation rate, using the formulas in Table XI-1, and taking n_{++}/n_+ from Fig. XI-2a. It is seen to be a marginal proposition to neglect this process, especially at high arc currents, when n_+ begins to decrease.

We can obtain an upper limit to the ratio of electron excitation from the resonance level to that from the ground state by assuming 100 per cent imprisonment and depopulation of the resonance level by ionization by electron impact. This ratio is

$$\frac{\beta_{1j} n_1}{\beta_{oj} n_o} = \frac{\beta_{1j}\beta_{o1}}{\beta_{oj}\beta_{1\infty}} = 10^{-3}\, e^{(V_\infty - V_1)/T_-}$$

(see Table XI-2). Incomplete imprisonment and other resonance level losses – particularly superelastic collisions – tend to decrease this ratio.

If we assume that the cascade level is populated only by electron excitation from the ground state and depopulated only by spontaneous emission, the ratio of cascade to excitation contributions to n_j is simply

$$\frac{A_{kj} n_k}{\beta_{oj} n_- n_o} = \frac{A_{kj}}{A_k}\, e^{-(V_k - V_j)/T_-}.$$

Now, A_{kj} is proportional to $(V_k - V_j)^3$, so we would expect the branching ratio A_{kj}/A_k to be close to one only for transitions at optical frequencies. Thus we let $V_k - V_j = 2^V$ in the comparison in Table XI-2. Again, we have a marginal situation, but the estimates are presumably on the high side.

6. Intensity Measurements

A Jarrell-Ash 0.5-meter scanning monochromator was used in measuring the intensities of the argon ion lines. In the initial survey runs, light from the entire arc was

Table XI-1. Values of population coefficients.

Coefficient	$T_- = 2^V$	4^V	6^V
$\beta_{oj} = 1.8 \times 10^{-10} T_-^{-1/2} e^{-20/T_-}$ cm^3/sec	5.8×10^{-15}	6.1×10^{-13}	2.6×10^{-12}
$\beta_{ij} = 1.8 \times 10^{-10} T^{-1/2} e^{-4/T_-}$	7.1×10^{-12}	3.31×10^{-11}	3.8×10^{-11}
$\beta_{jk} = 1.8 \times 10^{-10} T^{-1/2} e^{-3/T_-}$	2.8×10^{-11}	4.3×10^{-11}	4.5×10^{-11}
$\beta_{j\infty} = 1.8 \times 10^{-7} T^{-1/2} e^{-7.5/T_-}$	3.0×10^{-9}	1.4×10^{-8}	2.1×10^{-8}
$\alpha_j = 10^{-13} T_-^{-3/4}$ cm^3/sec	6.0×10^{-14}	3.5×10^{-14}	2.6×10^{-14}
A_{kj}, $A_j \sim 10^9$ sec^{-1}			
$\frac{1}{\tau_{dj}} \sim 10^2 - 10^4$ sec^{-1}			
$\frac{1}{\tau_{cj}} \sim 10^4$ sec^{-1}			

Table XI-2. Ratios of secondary processes to electronic excitation.

Ratio	$T_- = 2$	2.4	3
$\frac{\alpha_j n_\infty}{\beta_{oj} n_o} = 5.5 \times 10^{-4} T^{-1/4} e^{20/T_-} \frac{n_{++}}{n_+}$	.097	.24	.60
$\frac{\beta_{ij} n_1}{\beta_{oj} n_o} = 10^{-3} e^{11.5/T_-}$	.32	.12	.046
$\frac{A_{kj} n_k}{\beta_{oj} n_o n_-} = e^{-2/T_-}$	.37	.48	.51

allowed to fall on the entrance slit, which was perpendicular to, and approximately 2 feet from, the arc axis. Later, a system of collimating slits and mirrors was interposed between the arc and the monochromator. This arrangement, Fig. XI-3, takes a

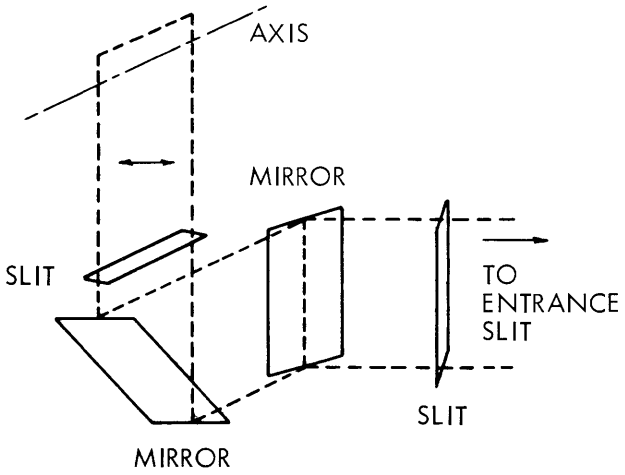

Fig. XI-3. Movable collimator.

narrow ribbon of light (0.005 in.) parallel to the arc axis and rotates it 90° so that it falls on the monochromator entrance slit. A lens was used to focus the light on the slit. The collimating-slit system is movable, scanning the arc perpendicular to the axis. No provision has been made for absolute intensity measurements; all measurements are in arbitrary units. A tungsten-ribbon filament lamp is being added to a new arrangement for calibration of intensities. The 1P21 photomultiplier output was amplified by a Philbrick UPA-2 operational amplifier, and displayed on a Varian G11A strip chart recorder. Often the intensity variation in one run would be large enough to necessitate changing the amplifier gain or photomultiplier voltage to keep the recorder on scale. In these cases, the run was made in overlapping segments, and the raw data were plotted on log paper. The gain factor was obtained from the displacement of the curves.

The measurements performed thus far have been on

(a) Light from the Whole Arc

(i) A spectrogram from 3200 Å to 5200 Å.

(ii) Intensity versus arc current for several ion lines.

(iii) Intensity versus magnetic field for several ion lines.

(b) Ribbon of Light (Arc Profiles)

(i) Arc profiles of several ion lines and many arc conditions.

(ii) Intensity on axis versus current.

A discussion of these measurements follows.

a. i. Approximately 30 AI, 190 AII, and 7 AIII lines have been identified out of more than 300 argon lines in a spectrogram taken at 20 amps and 800 gauss. All of the AI and AIII lines are rather weak compared with the most intense lines of the single ion. Twelve, out of 40, unidentified impurity lines had measurable, but very small, intensities. They are possibly Ta, Ne, or Fe lines, but the wavelengths are not precise enough for us to be sure. The intensity of the strongest impurity line (λ4580; Ta 4580.7 ?) is approximately 10^{-3} times the intensity of the stronges AII line (λ 4348).

Ion lines, strong enough to be of use, are listed below in order of increasing excitation potential.

V_x	λ	I (arb)	V_x	λ	I (arb)
19.14	4806	25,000	19.88	3851	9,550
19.18	4736	22,800	21.05	4609	16,600
19.41	4348	25,000	21.40	4370	11,800
19.46	4426	25,000	22.85	3588	5,400
19.88	3729	9,800	23.07	3868	1,670

a. ii. The intensities of λ4806, λ4736, λ4348, λ4426 are plotted in Fig. XI-4 as I_1, those of λ4370, λ3588 as I_2, all normalized to 100 at 65 amps. The magnetic field was 1200 gauss. The flow rate was 130 cc-atm/min which produced a pressure of 2-3 μ Hg in the arc tube. Although there is considerable scatter in the data points, there is a distinct difference between the intensities of lines originating at levels between 19.1 volts and 19.5 volts and those originating between 21.4 volts and 22.9 volts.

If we assume that the line intensities are given by

$$I_j = c_j n_- n_+ T^{-1/2} e^{-V_j/T} \qquad j = 1, 2,$$

and take logarithms of intensity ratios, we can see how T_- varies once it is known for one current setting. $V_2 - V_1$ is approximately equal to 3 volts. Taking ratios at 30, 65, and 100 amps, and assigning values to T_{100}, we obtain the values listed below

T_{30}	T_{65}	T_{100}
1.9	2.2	2.4
2.1	2.4	2.6
2.2	2.5	2.8
2.3	2.8	3.0
2.5	3.2	3.5
2.9	3.6	4.0

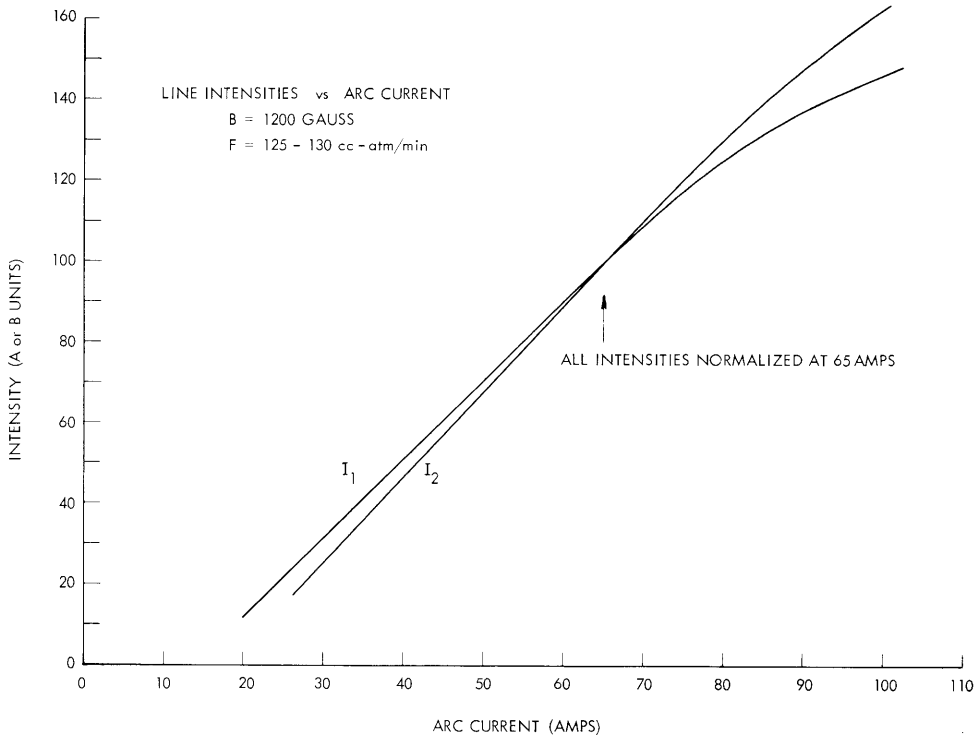

Fig. XI-4. Line intensities vs arc current.

The fact that the intensity of ion lines increases linearly with current is rather surprising, since it is proportional to electron density times ion ground-state density. Since, even at 30 amps, the concentration of n_{++} is great enough to produce significant AIII line intensity, it is probable that the arc is operating near the peak of the n_+ density. The slower increase in intensity at currents higher than 80 amps could then be explained by a depletion in n_+ density as n_{++} builds up; comparison of this table with Fig. XI-2 supports this hypothesis.

a. iii. All line intensities increased gradually as the magnetic field was increased from 1000 gauss to 2200 gauss, at 65 amps arc current. Total increase was appoximately a factor of 2, and no significant dependence on excitation potential could be discerned.

b. i. A typical profile is shown in Fig. XI-5. This curve is λ4348 at 50 amps, 1200 gauss, and 100 cc-atm/min (1-1.5 μ Hg in arc tube). The original idea in this experiment was to measure the radial variation of intensity for three lines with widely separated upper levels, for example, λ4348, λ4370, λ3868 at 19.4, 21.4, 23.1 volts, and deduce the radial variation in electron temperature, by comparing intensity ratios as we did in (a. ii). This experiment has not yielded useful results because accurate alignment of the monochromator could not be maintained because

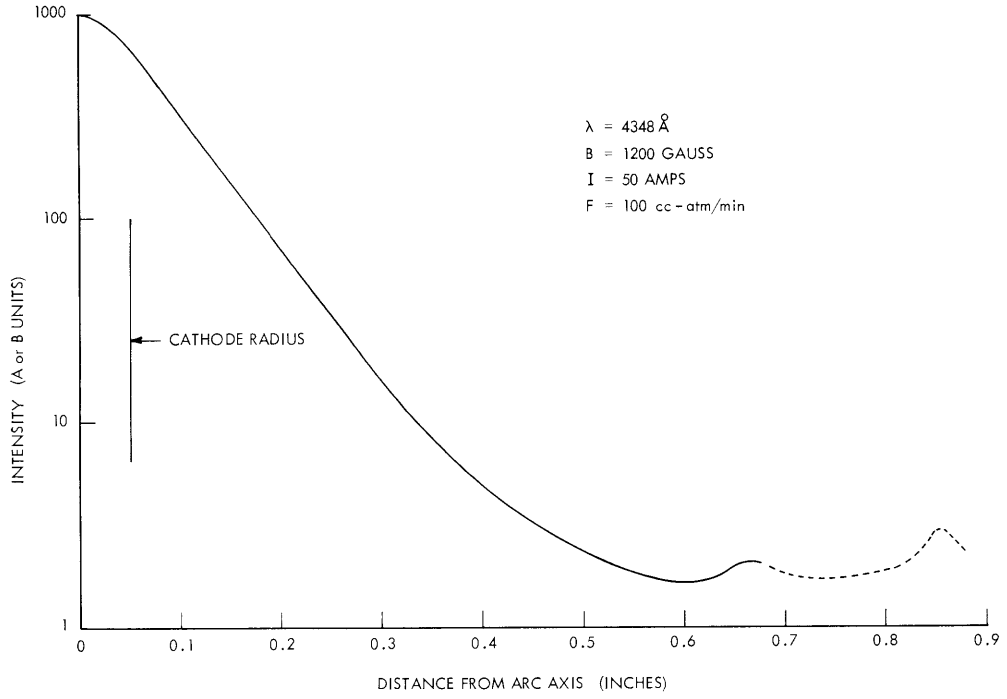

Fig. XI-5. Intensity of λ4348 vs distance from arc axis.

of vibration; also, the arc does not remain sufficiently constant from run to run.

A new monochromator and slit-system mount has been made to solve the alignment problem, and we shall try again. A moving probe is now being built which should sweep through the arc fast enough to enable density and other probe measurements without burning up. Once we know, from probe measurements, the plasma density profile, and the electron temperature close to the edge of the arc, we shall be able to use a single line intensity curve to obtain the temperature profile.

Two features of Fig. XI-3 are worth noting:

(i) The intensity falls off almost exponentially with distance from arc axis – not radius, as the data have not yet been inverted. The slope of the log I curve then affords a measure of the width of the arc column, as determined by diffusion. The variation of width (reciprocal of the slope) with magnetic field is shown for several conditions in Fig. XI-6. If anything, there seems to be an increase of a few per cent in width as B runs from 800 gauss to 2000 gauss. There is a much more pronounced increase as current and/or flow rate are increased, but no systematic measurements have been made.

(ii) The width of the crown – the portion from the axis to the exponential – is not determined solely by the cathode diameter. At higher pressure it broadens

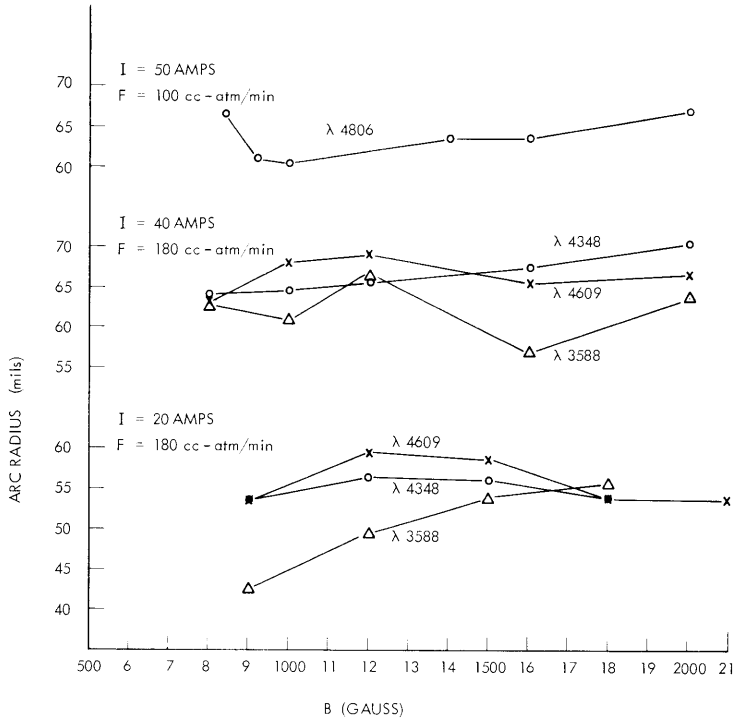

Fig. XI-6. Arc width vs magnetic field.

considerably and the exponentials are flatter. Also, we looked for a bump in this crown which might be due to excitation by primary electrons from the cathode. None was found within the resolution of the measurements, which is perhaps a few per cent near the intensity maxima. These observations lend further support to our general analysis, which assumes that all of the light is generated by plasma electrons rather than by a monoenergetic beam issuing from the cathode.

b. ii. Intensity versus current measurements have to be repeated with the collimating slit set on-axis because the alignment problem became worse when these measurements were made. Generally speaking, however, the intensity seems, first, to rise and then to drop off rather sharply as the current is increased. This indicates that the n_+ is markedly depleted, and n_{++} is considerably increased near the axis at high current.

C. D. Buntschuh

References

1. C. D. Buntschuh, Quarterly Progress Report No. 65, Research Laboratory of Electronics, M.I.T., April 15, 1962, pp. 79-87.

2. L. M. Lidsky, S. D. Rothleder, D. J. Rose, S. Yoshikawa, C. Michelson, and J. R. Mackin, Jr., J. Appl. Phys. 33, 2490 (1962).

3. H. S. W. Massey and E. H. S. Burhop, Electronic and Ionic Impact Phenomena (Oxford University Press, London, 1952).

4. T. Holstein, Phys. Rev. 72, 1212 (1947); 83, 1159 (1950).

5. R. Fowler, Radiation from Low-Pressure Discharges, Handbuch der Physik, Vol. 22, Edited by S. Flügge (Springer Verlag, Berlin, 1956), pp. 209-253.

B. INDIUM ANTIMONIDE PHOTODETECTOR FOR SUBMILLIMETRIC RADIATION

This photoconductive detector, purchased from Mullard Ltd., is sensitive to radiation from 100 μ to beyond 1 mm, and has a response time of less than 1 μsec. The InSb sample, located at the bottom of a vertical light pipe, is immersed in liquid helium. By pumping on the helium, the sample temperature is reduced to less than 1.6°K. The InSb operates in a 6 kgauss magnetic field obtained from a superconducting niobium solenoid.

The InSb detector was compared with a Golay cell. Both detectors were exposed to radiation from 200 μ to 300 μ, chopped at 15 cps. The signals from each detector were preamplified, and then synchronously detected. The signal-to-noise ratio of the InSb detector was approximately 25 times better than that of the Golay cell. Further improvement in signal-to-noise ratio has resulted from increasing the chopping frequency to 3100 cps, and from a corresponding decrease in preamplifier noise.

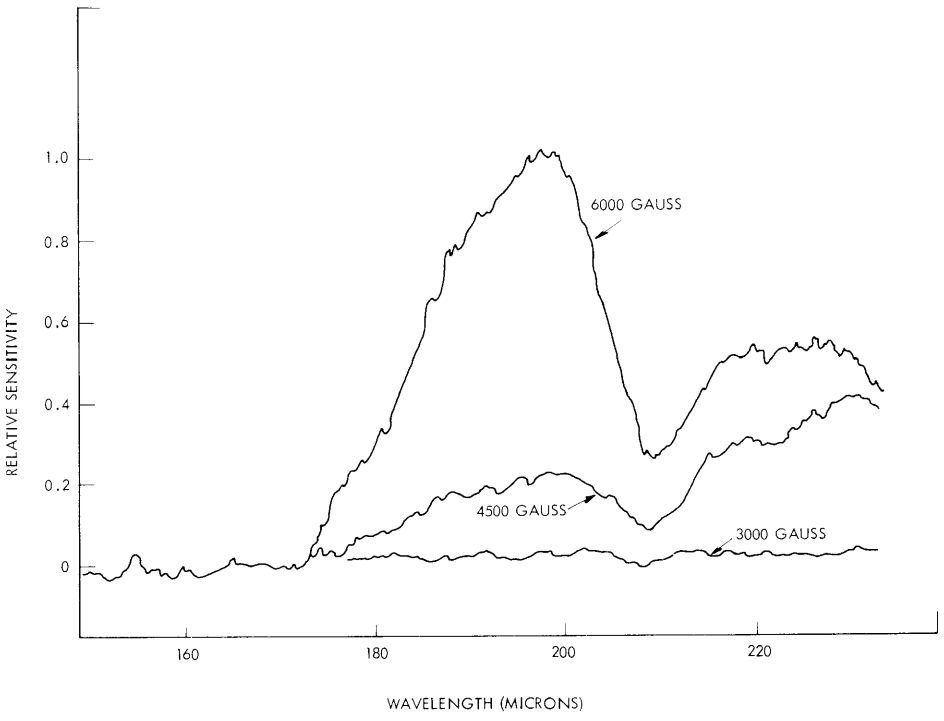

Fig. XI-7. InSb detector sensitivity as a function of wavelength magnetic field surrounding InSb sample varied from 3 kgauss to 6 kgauss.

The detector exhibited a short wavelength cutoff, as shown in Fig. XI-7, which is dependent on the magnetic field strength.

R. E. Whitney

C. PLASMA-WAVE COUPLING ANGLE

The dispersion relation for longitudinal plasma waves is

$$\left(\frac{A}{B-n^2}\right)_+ + \left(\frac{A}{B-n^2}\right)_- = 1. \tag{1}$$

Here, the plus and minus signs refer to ions and electrons.[1] The following definitions have been used: n is the refractive index, $A = \frac{\alpha^2}{\delta}$, $B = \frac{1-\beta^2}{(1-\beta^2\cos^2\theta)\,\delta}$, $\delta = \frac{kT}{mc^2}$, $\alpha^2 = \frac{\omega_p^2}{\omega^2}$, $\beta = \frac{\omega_b}{\omega}$, ω_p is the plasma frequency, ω_b is the cyclotron frequency, and θ is the angle between the propagation vector and the constant magnetic field. The ion flux and electron particle flux along the k vector, $\Gamma_\pm$, for the two modes of plasma waves are related by the expression,

$$\left(\frac{\Gamma_-}{\Gamma_+}\right)_1 \cdot \left(\frac{\Gamma_-}{\Gamma_+}\right)_2 = -\frac{T_+}{T_-}, \tag{2}$$

in which the numeral subscripts refer to the modes. Equation 2 states that if the electrons and ions vibrate in phase for one mode, they will be out of phase for the other. The angles for which the phase of vibration changes are the resonance angles given by

$$\tan^2\theta_R^+ = \beta_+^2 - 1, \qquad \tan^2\theta_R^- = \beta_-^2 - 1. \tag{3}$$

These results have been derived and discussed elsewhere.[1,2]

Equation 1 can be written in a form that displays the coupling of ion and electron waves:

$$\left(n^2+A_+-B_+\right)\left(n^2+A_--B_-\right) = A_+A_-. \tag{4}$$

If the coupling term, A_+A_-, is disregarded, an angle is determined at which the separated ion and electron waves intersect on a polar plot of phase velocity as a function of angle of propagation. One would suspect that this angle would indicate a region of strong coupling between the waves and therefore have physical significance. This coupling angle, θ_c, is defined as

$$A_+ - B_+ = A_- - B_-. \tag{5}$$

When ion and electron temperatures are equal, Eq. 5 simplifies considerably and yields

$$\tan^2 \theta_c = \frac{\left(\beta_-^2 - 1\right)\left(1 - \beta_+^2\right)}{1 + \beta_+\beta_-}. \tag{6}$$

Hence such a coupling angle will exist only between the cyclotron lines of the a^2, β^2 plane.[2]

If we consider the kinetic energy density (W) caused by motion along the propagation direction, that is,

$$W = \frac{m\Gamma^2}{2N_o} = \frac{1}{a^2}\left(\frac{A}{B - n^2}\right)^2 \frac{E_k^2}{8\pi}, \tag{7}$$

where $\Gamma^2 = \frac{\Gamma\Gamma^*}{2}$, and $\frac{E_k^2}{8\pi}$ is the energy density of the longitudinal electric field, and make use of Eq. 2, we obtain

$$\left(\frac{W_-}{W_+}\right)_1 \left(\frac{W_-}{W_+}\right)_2 = \left(\frac{\delta_+}{\delta_-}\right)^2. \tag{8}$$

In the very special case $\delta_+ = \delta_-$, that is, for equal electron and ion thermal velocities, Eq. 8 states that when the ions dominate the longitudinal kinetic energy of one mode, the electrons will dominate the other. For this case, the angle at which the kinetic energies of a particular mode change from electron- to ion-dominated will be the coupling angle θ_c. In the general case, however, there is no sharp distinction in the kinetic energy of the modes.

We shall now examine the potential energy density (which has been given by Allis, Buchsbaum, and Bers[3]):

$$\phi = \frac{1}{4}\frac{mV_T^2}{N_o} N_1 N_1^* = \frac{1}{4}\frac{mV_T^2}{N_o}\left(\frac{k}{\omega}\right)^2 \Gamma_k \Gamma_k^*, \tag{9}$$

where V_T is the thermal velocity; ϕ is $-\frac{P \cdot \delta V^*}{2V}$, with $P = N_1 kT \equiv 1/2 N_2 mV_T^2$, the pressure, and $\frac{\delta V}{V} = -\frac{N_2}{N_o}$ the fractional volume change.

Again using Eq. 2, we find the following relation for potential energies:

$$\left(\frac{\phi_-}{\phi_+}\right)_1 \left(\frac{\phi_-}{\phi_+}\right)_2 = 1. \tag{10}$$

Equation 10 indicates that if the potential energy is ion-dominated for one mode, it will be electron-dominated for the second mode. Furthermore, if we set $\phi_+ = \phi_-$, we find from Eqs. 7 and 9 that

$$n^4 + 2n^2\left[\frac{A_+B_- - A_-B_+}{A_- - A_+}\right] + \frac{A_-B_+^2 - A_+B_-^2}{A_- - A_+} = 0. \tag{11}$$

Equation 4 when written as a quadratic in n^2 is

$$n^4 + n^2[A_- + A_+ - B_- - B_+] + B_-B_+ - B_+A_- - B_-A_+ = 0. \tag{12}$$

Equating either the constant or middle coefficients of Eqs. 11 and 12 results in Eq. 5. Therefore, the potential-energy interchange occurs at the coupling angle. Thus a physical interpretation has been found for the geometrical coupling between the independent electron and ion plasma waves.

H. R. Radoski

References

1. H. R. Radoski, Dispersion relation for longitudinal plasma waves, Quarterly Progress Report No. 66, Research Laboratory of Electronics, M.I.T., July 15, 1962, p. 100.

2. W. P. Allis, S. J. Buchsbaum, and A. Bers, Waves in Anisotropic Plasmas (The M.I.T. Press, Cambridge, Mass., 1963), Chapter 5.

3. Ibid., Chapter 8, p. 119.